INTERNATIONAL JOURNAL FOR NUMERICAL METHODS IN FLUIDS
Int. J. Numer. Meth. Fluids 2003; **42**:1087–1103 (DOI: 10.1002/fld.579)

Numerical simulation of time-dependent hydrodynamic removal of a contaminated fluid from a cavity

Lih-Chuan Fang[1,*], Dimitri Nicolaou[2] and John W. Cleaver[2]

[1]*Department of Mechanical Engineering, Chinese Military Academy, P.O. Box 90602-6, Fengshan, Kaohsiung 830, Taiwan, ROC*
[2]*Department of Engineering, The University of Liverpool, Mechanical Engineering Building, Brownlow Street, L69 3GH, U.K.*

SUMMARY

The time-dependent hydrodynamic removal of a contaminated fluid from a rectangular cavity on the floor of a duct is analysed numerically. Laminar duct flows are considered for Reynolds numbers of 50 and 1600 where the characteristic length is the duct height. Two cases are considered where: (1) the fluid density in the cavity is the same as that for the duct fluid and (2) the cavity fluid has a higher density than the duct fluid but the two fluids are miscible. The flow is solved by a numerical solution of the time-dependent Navier–Stokes equations. Attention is focused on the convective transport of contaminated fluid out from the cavity and the effect of duct flow velocity profile on the cleaning process. Passive markers are used in the numerical simulation for the purpose of identifying the contaminated cavity fluid. The results show that the flow patterns in the cavity are influenced by the type of duct flow. From a cleaning perspective, the results suggest that it is easier for the duct flow to penetrate a cavity and to remove contaminated cavity fluid when the duct flow is of the Poiseuille type and the aspect ratio is large. Copyright © 2003 John Wiley & Sons, Ltd.

KEY WORDS: cavity; numerical; Navier–Stokes; hydrodynamic; miscible

1. INTRODUCTION

In the processing industry, the residues of industrial manufacturing processes can give rise to an accumulation of deposits in cavities of rough surfaces and consequently a corresponding degradation of quality in the processed material may be observed. The cavities may be formed by poorly fitted components and junctions in pipe work or ducts. For example, in the chemical and food processing industry, surfaces in ducts or pipelines are often fouled by the product or contaminant substance. This may cause a reduction in the performance of heat exchanger elements, increase in pressure losses and also result in adverse hygiene conditions arising.

*Correspondence to: Lih-Chuan Fang, Department of Mechanical Engineering, Chinese Military Academy, P.O. Box 90602-6, Fengshan, Kaohsiung 830, Taiwan, ROC.
†E-mail: lcfang@cc.cma.edu.tw

Copyright © 2003 John Wiley & Sons, Ltd.
Received August 2001
Revised 23 December 2002

The quality of the processed material is maintained by periodically cleaning the ducts and pipelines. The most common means of cleaning is to flush the system with an appropriate fluid which may be a solvent. Little published work is available to quantify the efficiency of the hydrodynamic removal of contaminated deposits suspended in fluid trapped in cavities. It is desirable to know under what conditions the cleaning of the cavity can be made more efficient.

Since flow separation occurs whenever there is an abrupt change of geometrical configuration of the body surface, and a good example of this is when a duct flow passes a cavity, numerous studies of flow over cavities have been motivated by a fundamental interest in the phenomenon of separated flow. Sometimes the separation streamline, which originates at the upstream corner, is reattached to the solid surface downstream and also encloses a re-circulation region. Many authors have reported their studies on this problem including Takematsu [1], Mehta and Lavan [2], O'Brien [3], Shen and Floryan [4], Higdon [5], Taneda [6] and Pozrikidis [7]. One key result from these studies is that the separation streamline and the intensity of the closed flow within the cavity are a function of cavity aspect ratio, relative duct size to cavity size, and the velocity profile within the duct. The important re-circulation regions play a major role in the problem of cavity cleaning. From a cleaning perspective, there is a reasonable presumption that foulant trapped in the re-circulating vortices will be difficult to remove.

Additional work regarding the mass transfer in a cavity has been presented in literature since the 1980s. Kang and Chang [8], Kim *et al.* [9] and Chang *et al.* [10] showed that the enhancement of mass transfer by vortices induced in a cavity due to external duct flow increases as cavity aspect ratio increases. Alkire and Reiser [11] and Alkire and Deligianni [12] investigated the effect of fluid flow on the removal of dissolution products from cavities of invariant shapes and of different aspect ratios. They showed that the small sizes of the cavities were not influenced by the type of external flow. As the cavity size increases, transport by convection will eventually predominate over diffusion processes. Yeckel *et al.* [13] and Mickaily *et al.* [14] developed a hydrodynamic model to study numerically the effect of periodic roughness on the duct flows. They demonstrated that the reduction in flow can be quantified as a function of well-defined surface roughness parameters for periodic surfaces.

Most previous studies have assumed that the velocity components in the cavity are those which exist in steady-state conditions. Recently Fang *et al.* [15] presented a numerical and experimental study of the transient removal of a contaminated fluid from a cavity on the floor of a duct. The results suggest that the cleaning of the foulant in a cavity with fluid of the same density as the fluid in the duct is more pronounced during the unsteady start-up of the duct flow, and the rate of cleaning decreases as the flow reaches a steady state. The cleaning process is enhanced as the cavity aspect ratio is increased and as the duct Reynolds number increases.

Chilukuri and Middleman [16] considered hydrodynamic cleaning of a surface by the use of a brush, a mop or a rotating drum. In these situations the layer of fluid between the solid surface and applicator is quite small and the flow between the applicator and the surface can be considered as Couette flow. Because of the small gap, the flow will also be laminar in nature. Some previous studies have focused on Couette flow over a cavity in which the upper wall of the duct is moved with a constant velocity. Examples are the studies by Mehta and Lavan [2], O'Brien [3] and Mickaily *et al.* [14]. They showed that there is a slightly different

Copyright © 2003 John Wiley & Sons, Ltd.

dividing streamline and cavity flow pattern between Poiseuille flow and Couette flow. Hence, it is of interest to know how the foulant is removed in Couette flow and how it might differ from Poiseuille flow.

In the present study the flow is always considered to be laminar. Two cases are considered where the density of the cavity fluid is concerned. First, the cavity fluid density, in which the contaminant particles are suspended, is taken to be the same as the density of the fluid in the duct. The second case considers two miscible fluids, the density of the fluid in the cavity being higher than the density of the fluid flowing through the duct. Therefore, the study of hydrodynamic removal involves unsteady separated flow and mass transfer via convection and diffusion.

The numerical method used to solve governing fluid flow equations is based on the marker and cell (MAC) method of Harlow and Welch [17]. Passive markers are used to visualize the flow and to quantify the hydrodynamic cleaning of the cavities. Similar finite difference formulations of the equations of motion for other problems have been used previously by, among others, Miyata and Nishimura [18], Liu *et al.* [19], and Nicolaou *et al.* [20, 21]. These studies which cover a variety of fluid flow problems show that the formulation works well for modelling incompressible laminar flows. The computer code which has been written for the present investigation has been validated by calculating and comparing lid-driven cavity flows with results of previous studies; the validation results are given by Fang *et al.* [15].

2. PHYSICAL MODEL AND NUMERICAL METHOD

The geometry of the duct-cavity configuration employed in this study is shown in Figure 1. A Cartesian co-ordinate system is used with origin at the lower left-hand corner of the computational domain. The cavity dimensions are defined by width W and depth D. A cavity aspect ratio, AR, is defined by the ratio W/D. Fluid of density ρ and viscosity μ flows continuously into the duct from the left and exits on the right. The acceleration due to gravity, g, acts in the negative z direction. All solid boundaries are assumed to be rigid no-slip walls. The height of the duct H was kept constant. Preliminary numerical experiments have indicated that entry lengths of twice the duct height ($2H$) or greater cause negligible changes in the results and therefore it has been considered sufficient to use entry lengths of $2H$ for all the cases considered.

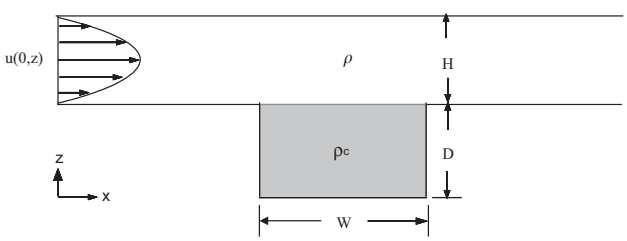

Figure 1. The geometry of the duct and cavity, and the co-ordinate system.

Copyright © 2003 John Wiley & Sons, Ltd.

The maximum inlet velocity U and duct height H are used to define non-dimensional velocities (u,w), spatial co-ordinates (x,z), time (t) and pressure (p) which are given by

$$u=\bar{u}/U, \quad w=\bar{w}/U, \quad x=\bar{x}/H, \quad z=\bar{z}/H, \quad t=U\bar{t}/H \quad \text{and} \quad p=\bar{p}/\bar{\rho}U^2$$

where a bar represents the corresponding dimensional quantity and $\bar{\rho}$ is fluid density. The fundamental non-dimensional equations in Cartesian form for two-dimensional incompressible flow of a Newtonian fluid with constant properties are:

$$\frac{\partial \rho u}{\partial t}+\frac{\partial(\rho u^2)}{\partial x}+\frac{\partial(\rho uw)}{\partial z}=-\frac{\partial p}{\partial x}+\frac{1}{Re}\left(\frac{\partial^2 u}{\partial x^2}+\frac{\partial^2 u}{\partial z^2}\right) \tag{1}$$

$$\frac{\partial \rho w}{\partial t}+\frac{\partial(\rho wu)}{\partial x}+\frac{\partial(\rho w^2)}{\partial z}=-\frac{\partial p}{\partial z}+\frac{1}{Re}\left(\frac{\partial^2 w}{\partial x^2}+\frac{\partial^2 w}{\partial z^2}\right)-(\rho-\rho_s)Fr^{-2} \tag{2}$$

$$\frac{\partial \rho}{\partial t}+\frac{\partial \rho u}{\partial x}+\frac{\partial \rho w}{\partial z}=Di\left[\frac{\partial^2 \rho}{\partial x^2}+\frac{\partial^2 \rho}{\partial z^2}\right] \tag{3}$$

$$\frac{\partial u}{\partial x}+\frac{\partial w}{\partial z}=0 \tag{4}$$

where $Re=UH/v$ is the Reynolds number, $Fr=U/(gH)^{1/2}$ is Froude number, and $Di=\mathsf{D}/UH$ is a constant in which D is the coefficient of diffusivity. The hydrostatic pressure and density distributions have been subtracted from the equations so p and $(\rho-\rho_s)$ represent the perturbation pressure and density values, respectively, where ρ_s is the static distribution of density at $t=0$.

The flow field is divided into cells of size $\delta x\times\delta z$ with cell centres being designated by indices i in the x direction and k in the z direction. The horizontal velocity component, u, is located on the vertical sides of the cell, and the vertical velocity component, w, is located on the horizontal upper and lower sides of each cell. The pressure p and density ρ are located at the cell centres. The Navier–Stokes equations are represented in a finite-difference form by forward differencing in time and centred differencing in space, except for the convection terms where a combination of centred and upstream differencing is used. For example, if integer 'n' represents the time level, then u at a new $(n+1)$ time level is calculated from

$$(\rho u)^{n+1}_{i+1/2,k}=\eta_{i+1/2,k}-\frac{\delta t}{\delta x}(p^{n+1}_{i+1,k}-p^{n+1}_{i,k}) \tag{5}$$

where

$$\begin{aligned}\eta_{i+1/2,k}=(\rho u)_{i+1/2,k}&-\delta t(UXX_{i+1/2,k}+UXZ_{i+1/2,k})\\&+\frac{\delta t}{\delta x^2}Re^{-1}(u_{i+3/2,k}-2u_{i+1/2,k}+u_{i-1/2,k})\\&+\frac{\delta t}{\delta z^2}Re^{-1}(u_{i+1/2,k+1}-2u_{i+1/2,k}+u_{i+1/2,k-1})\end{aligned}$$

Copyright © 2003 John Wiley & Sons, Ltd.

The convection terms in (5) are given by

$$UXX_{i+1/2,k} = \frac{1}{4\delta x}\{\rho_{i+1,k}[(u_{i+3/2,k} + u_{i+1/2,k})^2 - \alpha|u_{i+3/2,k} + u_{i+1/2,k}|(u_{i+3/2,k} - u_{i+1/2,k})]$$
$$-\rho_{i,k}[(u_{i+1/2,k} + u_{i-1/2,k})^2 - \alpha|u_{i+1/2,k} + u_{i-1/2,k}|(u_{i+1/2,k} - u_{i-1/2,k})]\}$$
$$UXZ_{i+1/2,k} = \frac{1}{4\delta z}\{\rho_{i+1/2,k+1/2}[(w_{i,k+1/2} + w_{i+1,k+1/2})(u_{i+1/2,k} + u_{i+1/2,k+1})$$
$$-\alpha|w_{i,k+1/2} + w_{i+1,k+1/2}|(u_{i+1/2,k+1} - u_{i+1/2,k})]$$
$$-\rho_{i+1/2,k-1/2}[(w_{i+1,k-1/2} + w_{i,k-1/2})(u_{i+1/2,k-1} + u_{i+1/2,k})$$
$$-\alpha|w_{i,k-1/2} + w_{i+1,k-1/2}|(u_{i+1/2,k} - u_{i+1/2,k-1})]\}$$

where α is a combination factor. $\alpha = 0$ gives centred differencing and $\alpha = 1$ gives upstream differencing. Approximate stability conditions for the iteration procedure are given by Miyata and Nishimura [18]:

$$\left(\frac{\delta t}{\delta x}u + \frac{\delta t}{\delta z}w\right) \leqslant \alpha \leqslant 1 \tag{6}$$

and

$$v \leqslant \frac{1 - \alpha(\delta t/\delta x u + \delta t/\delta z w)}{2\delta t(1/\delta x^2 + 1/\delta z^2)} \tag{7}$$

Equation (6) gives conditions for the combination factor and the Courant number, and it limits the distance a fluid particle can travel in one time step to the smallest side of a cell. Equation (7) represents an upper limit on viscosity and it is important when highly viscous flows are being considered.

The combined upstream-centred differencing scheme introduces a variable amount of artificial diffusion useful in overcoming the destabilizing negative diffusion present in pure centred differencing schemes. Several tests using a collapsing uniform density region in a stratified flow have shown that a value of 0.5 provides sufficient positive numerical diffusion to overcome the instabilities arising from numerically introduced negative diffusion without significantly affecting the physics of the flow.

The solution procedure is based on the artificial compressibility method of Chorin [22] and involves a simultaneous iteration on pressure and velocity component. If $D_{i,k}^{n+1}$ represents the divergence of the fluid in a cell, where

$$D_{i,k}^{n+1} = \frac{1}{\delta x}(u_{i+1/2,k}^{n+1} - u_{i-1/2,k}^{n+1}) + \frac{1}{\delta z}(w_{i,k+1/2}^{n+1} - w_{i,k-1/2}^{n+1}) \tag{8}$$

then the pressure in cell (i, k) is updated through

$$(p_{i,k}^{n+1})^{m+1} = (p_{i,k}^{n+1})^m - R_f(D_{i,k}^{n+1})^m$$

Copyright © 2003 John Wiley & Sons, Ltd.

where m is an iteration count and R_f is a relaxation parameter. The four velocities in Equation (8) involve five pressure terms: $p_{i,k}^{n+1}$, $p_{i+1,k}^{n+1}$, $p_{i-1,k}^{n+1}$, $p_{i,k+1}^{n+1}$ and $p_{i,k-1}^{n+1}$. $(p_{i-1,k}^{n+1})^m$ and $(p_{i,k-1}^{n+1})^m$ can be replaced by the values from the latest iteration $(p_{i-1,k}^{n+1})^{m+1}$ and $(p_{i,k-1}^{n+1})^{m+1}$ while sweeping in the direction of increasing i and k This minimizes the number of iterations required for convergence. The stability restriction is given by $R_f \leqslant \rho\delta x^2/2\delta t$ [23]. The optimum value of R_f giving the most rapid convergence can, in general, only be determined by experimentation. Usually it is around $R_f = 1.8$. The solution is reached when the magnitude of $D_{i,k}^{n+1}$ in each cell is less than some pre-set small value, typically $O(10^{-6})$. When the velocity–pressure iteration has converged, the density is updated using

$$\rho_{i,k}^{n+1} = \rho_{i,k} - \frac{\delta t}{2\delta x}(\rho_{i+1,k}^{n+1}u_{i+1/2,k}^{n+1} - \rho_{i-1,k}^{n+1}u_{i-1/2,k}^{n+1}) - \frac{\delta t}{2\delta z}(\rho_{i,k+1}^{n+1}u_{i,k+1/2}^{n+1} - \rho_{i,k-1}^{n+1}u_{i,k-1/2}^{n+1})$$
$$-\frac{\delta t}{2}\rho_{i,k}^{n+1}D_{i,k}^{n+1} + Di\left(\frac{\rho_{i+1,k}^{n+1} - 2\rho_{i,k}^{n+1} + \rho_{i-1,k}^{n+1}}{\delta x^2} + \frac{\rho_{i,k+1}^{n+1} - 2\rho_{i,k}^{n+1} + \rho_{i,k-1}^{n+1}}{\delta z^2}\right) \tag{9}$$

The entire solution is considered to reach the convergence when the change in density is not greater than a small value ε_ρ given by

$$|(\rho_{i,k}^{n+1})^{r+1} - (\rho_{i,k}^{n+1})^r|_{\max} < \varepsilon_\rho$$

The superscript r is a density calculation iteration count which is increased by one each time the density is updated. If the density change in all cells is greater than ε_ρ, then the velocity–pressure fields are updated and the procedure is repeated.

The density equation (9) is used only when there is a density difference between the fluid in the cavity and the fluid in the duct; otherwise the density is kept constant. The density equation provides the mechanism by which mass transfer occurs between the higher density cavity fluid and the fluid in the duct. The diffusion term is usually negligible for smoothly varying densities, but may be significant when a sharp density interface exists. For example, during the initial stages of a duct flow over a cavity containing a heavier, miscible fluid. The effects of diffusion may also dominate over very long periods of time after convection becomes negligible. The density equation plays no direct role in the transport of the suspended contaminants in the fluid represented by the passive marker particles, but only through the flow induced due to diffusion. That is, Equation (9) is not a species equation. For the type of problem considered in the present study where the difference in density is assumed to be due to a saline solution in the cavity, the constant of diffusivity, D, has the approximate value of $1.3 \times 10^{-9}\,\mathrm{m}^2/\mathrm{s}$. This corresponds to sea water at a temperature of 20°C.

The computational mesh is surrounded by a one-cell-thick layer of cells, which are used for setting boundary conditions. No-slip boundary conditions are applied at all solid boundaries, a flow velocity is prescribed at the inflow boundary and zero normal gradients are used to set variables just outside the outflow boundary.

Flow visualization and fluid contamination calculations are made possible by the use of passive markers. These are initially distributed before start-up and are moved to new positions at each time step. For example the new x-position at time level $n+1$ of a marker identified by the index k is calculated from $x_k^{n+1} = x_k^n + u_k^{n+1}\delta t$ where u_k is the horizontal velocity at the marker position, x_k^n. The velocity components at the marker positions are calculated

Copyright © 2003 John Wiley & Sons, Ltd.

by a weighted interpolation of velocities from the surrounding cells as described by Welch *et al.* [24].

The computational mesh resolution was chosen by successively reducing the cell size until the effect on the results relating to cavity cleaning was negligible. Smaller cell sizes did improve the resolution of the smaller coherent structures in the flow such as the small corner vortices. The cell size used for all the numerical calculations was 0.02×0.02. Based on this cell size and the flow speed in the duct, a time step was used that satisfied Equation (6) for $\alpha = 0.5$. The time step used never exceeded $\delta t = 0.01$ for the range of Reynolds numbers considered.

3. RESULTS AND DISCUSSION

3.1. Case 1: Cavity fluid density equals duct fluid density

Figure 2 shows the streamlines for Poiseuille duct flow over cavities of different aspect ratios (width/depth) in the range AR = 0.25–4.0. The Reynolds number of the duct flow is $Re = 50$ and the figures show the flow when the steady state has been reached. Figures 2(a)–2(c) show cavities with AR equal to or greater than 1.0 formed by keeping the cavity depth constant, and equal to the duct height, while the cavity width is varied. For Figure 2(d) the cavity depth is

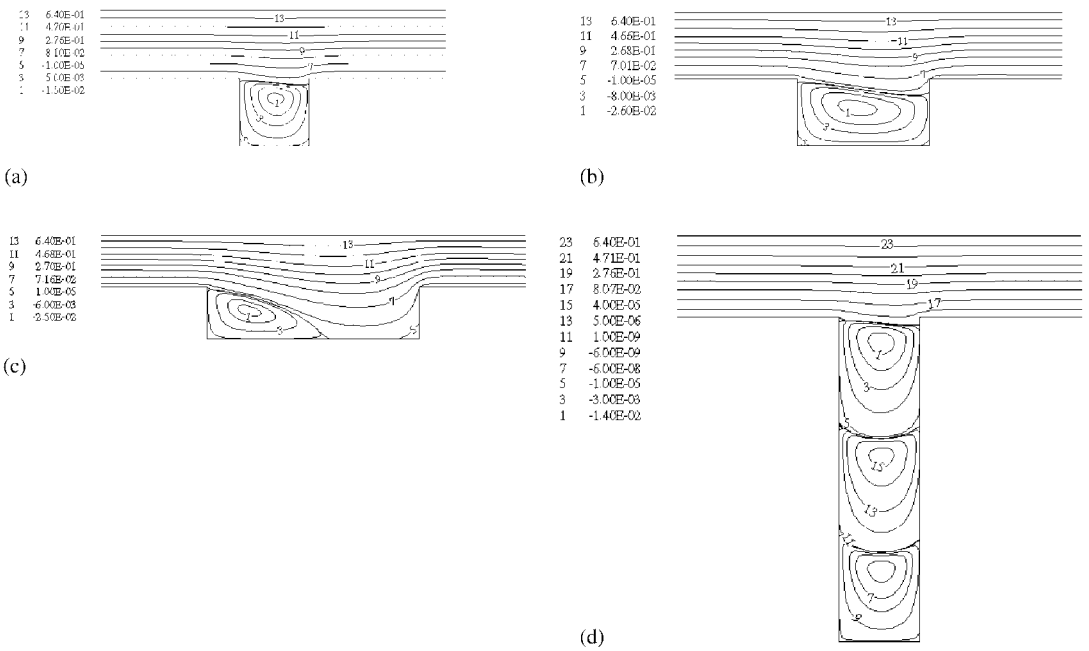

Figure 2. Steady-state streamlines of Poiseuille flow over cavities for $Fr = 0.0086$, $Di = 0$, $Re = 50$. Legend gives non-dimensional stream function values. (a) AR = 1.0; (b) AR = 2.0; (c) AR = 4.0 and (d) AR = 0.25.

Copyright © 2003 John Wiley & Sons, Ltd.

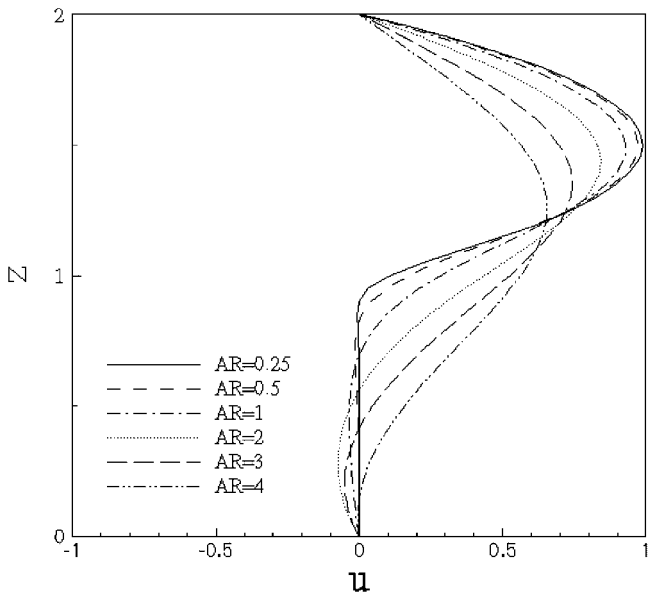

Figure 3. Steady-state normalized velocity profiles at cavity mid-width location for various cavity aspect ratios. Duct flow type: Poiseuille. $Fr = 0.0086$, $Di = 0$, $Re = 50$.

four times the cavity width and the duct height is equal to the cavity width. After steady-state conditions have been reached the square cavity, AR = 1, contains a single dominant large vortex which occupies most of the cavity. For AR = 2.0, the outer flow penetrates into the cavity at the downstream end of the cavity, but the penetration does not reach the bottom of the cavity. The widest cavity considered, corresponding to an aspect ratio AR = 4.0, has the duct flow penetrating to the bottom of the cavity leaving one large main vortex and a small isolated vortex in the corner. For a deep cavity, with AR = 0.25, three main vortices are formed in the cavity. The velocity profiles at the mid-width location in the cavity for a range of AR values when $Re = 50$ are shown in Figure 3. Clearly, the higher velocities occur for AR = 4.0, a consequence of the more pronounced penetration of the duct flow into the cavity.

Couette duct flow over a cavity, shown in Figure 4, does not significantly alter the flow patterns for the AR = 1 and 0.25 cavities. However, significant differences between Couette flow and Poiseuille flow are shown in the wider cavities with AR = 2.0 and 4.0. Couette duct flow does not penetrate deep into the cavity, even for these larger cavity aspect ratios; furthermore, the dividing streamline can bulge out into the duct as the cavity aspect ratio increases. Figure 5 shows the velocity profiles in a cavity corresponding to Couette duct flow. Different AR are considered for a fixed Reynolds number of 50. In contrast to Poiseuille duct flow, the cavity flows are predominantly circulatory, even for the larger aspect ratios. The magnitudes of the velocities in the cavity are substantially lower than those for Poiseuille flow.

A measure of the cleaning effectiveness of cavities of different aspect ratios can be determined using an area fraction approach. This involves calculating the area fraction of re-circulating fluid in the cavity. Figure 6 shows the fraction of the cavity area containing contaminated fluid when the flow reaches its steady state. The parameter A_ψ/A_c is roughly

Copyright © 2003 John Wiley & Sons, Ltd.

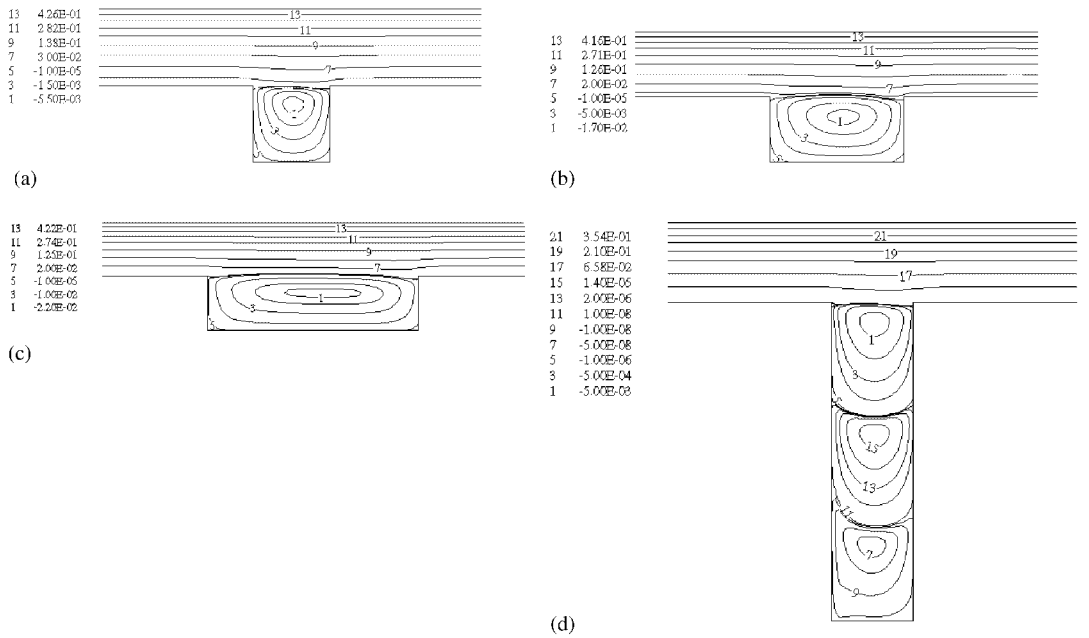

Figure 4. Steady-state streamlines of Couette flow over cavities for $Fr = 0.0086$, $Di = 0$, $Re = 50$. Legend gives non-dimensional stream function values. (a) AR = 1.0; (b) AR = 2.0; (c) AR = 4.0 and (d) AR = 0.25.

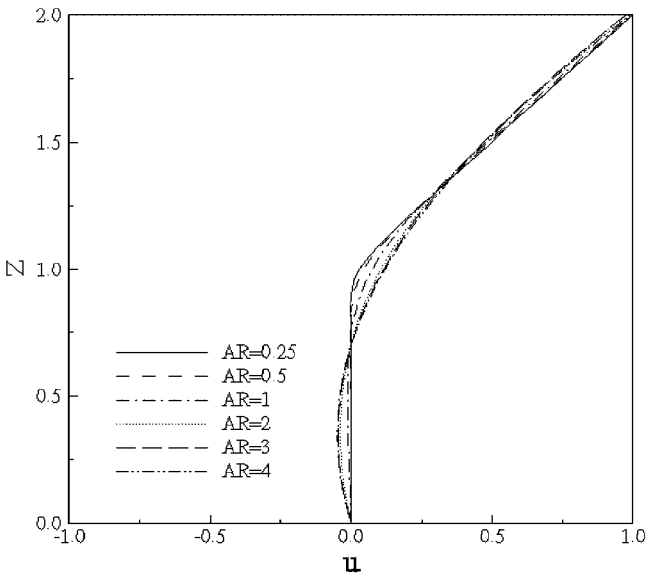

Figure 5. Steady-state normalized velocity profiles at cavity mid-width location for various cavity aspect ratios. Duct flow type: Couette. $Fr = 0.0086$, $Di = 0$, $Re = 50$.

Copyright © 2003 John Wiley & Sons, Ltd.

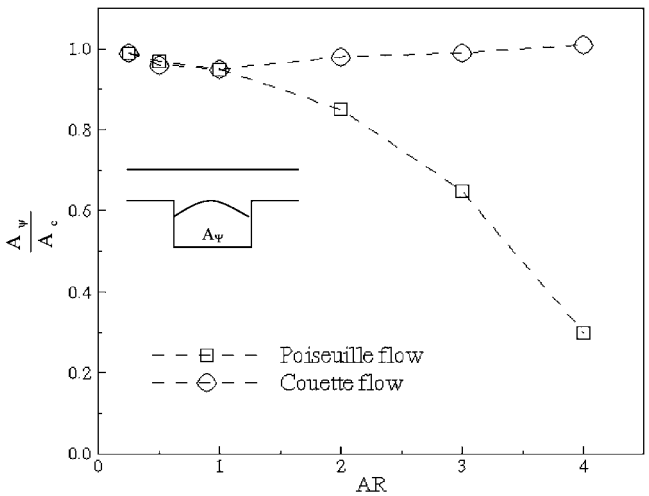

Figure 6. Area fraction of fluid trapped in cavities against cavity aspect ratio. $Fr = 0.0086$, $Di = 0$, $Re = 50$.

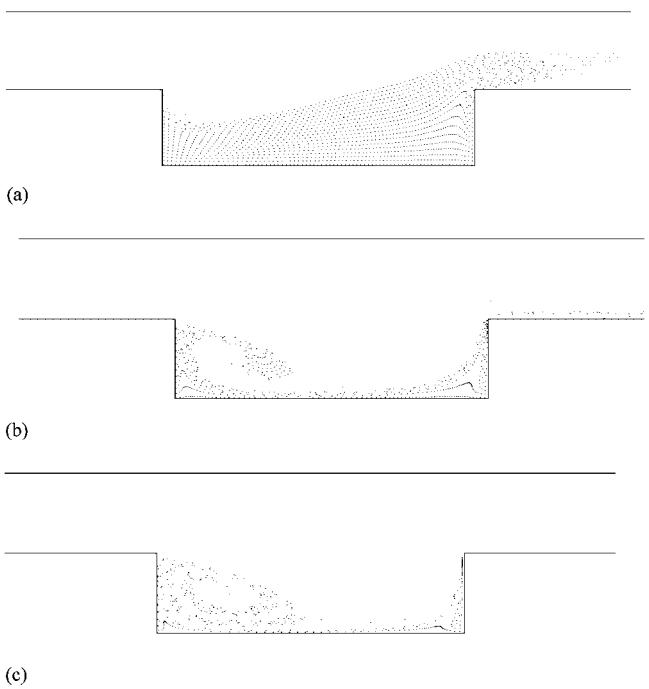

Figure 7. Flow development in a cavity of AR = 4 corresponding to Poiseuille flow in the duct. $Fr = 0.0086$, $Di = 0$, $Re = 50$. (a) $t = 6$; (b) $t = 32$ and (c) $t = 64$.

Copyright © 2003 John Wiley & Sons, Ltd.

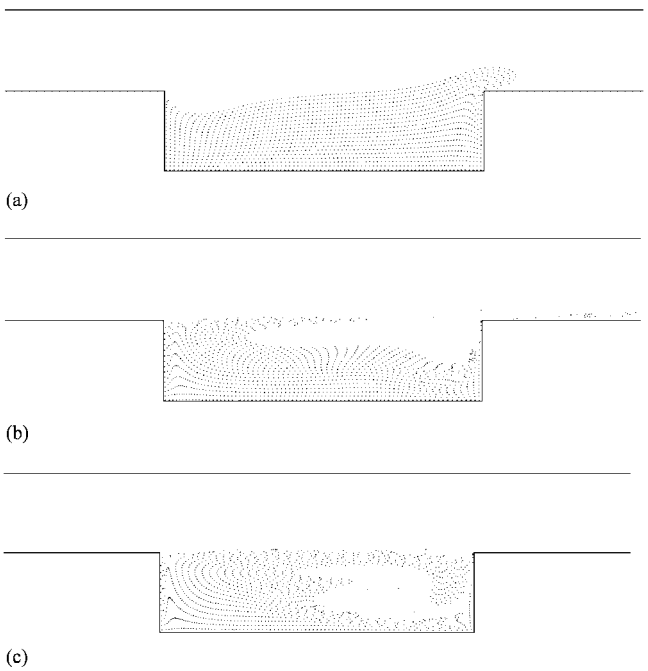

Figure 8. Time-dependent flow development in a cavity of AR = 4 corresponding to Couette duct flow. $Fr = 0.0086$, $Di = 0$, $Re = 50$. (a) $t = 6$; (b) $t = 32$ and (c) $t = 64$.

a measure of the fraction of fluid re-circulation in the cavity, where A_ψ represents the area of the re-circulating flow (see inset in Figure 6) and A_c presents the total area of the cavity. The extent of penetration of duct flow into the cavity is related to the value of A_ψ/A_c. When A_ψ/A_c is less than unity, the duct flow penetrates the cavity. When A_ψ/A_c is equal to or exceeds unity, then the re-circulating flow will occupy the whole cavity and can, under certain conditions, also bulge into the duct flow. For Poiseuille flow, the value of A_ψ/A_c increases with decreasing cavity aspect ratio. That is, for deep cavities more fluid is confined in the cavity space.

In the context of cavity cleaning via hydrodynamic removal, the onset of regions of re-circulating flow inside a cavity prevents the fresh duct water from reaching the deepest regions of the cavity and thus contaminant removal is hindered. The observations for Poiseuille flow is that the cavity area covered by re-circulating flow decreases with increasing cavity aspect ratio and therefore the duct flow penetrating into the cavity is made easier. For Couette flow, the value of A_ψ/A_c can be larger than unity and is little affected by cavity aspect ratio. The penetration of the duct flow into the cavity is severely restricted and the contaminant is effectively trapped in the cavity.

Although the hydrodynamic model developed by Yeckel *et al.* [13] and Mickaily *et al.* [14] is able to predict how much fluid is eventually trapped in a cavity, the streamline patterns within a cavity do not indicate to what extent the original cavity fluid is displaced by fresh fluid from the duct. To assess how fluid is purged from the cavity a 1600 markers are evenly distributed in the cavity prior to initiating the flow. Figure 7 shows how the markers in the

Copyright © 2003 John Wiley & Sons, Ltd.

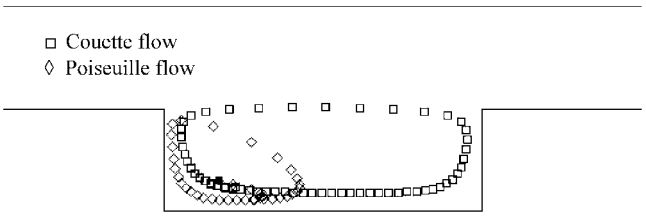

Figure 9. Single marker path for Couette and Poiseuille flows. The filled symbol indicates the starting point. AR = 4, $Fr = 0.0086$, $Di = 0$ and $Re = 50$.

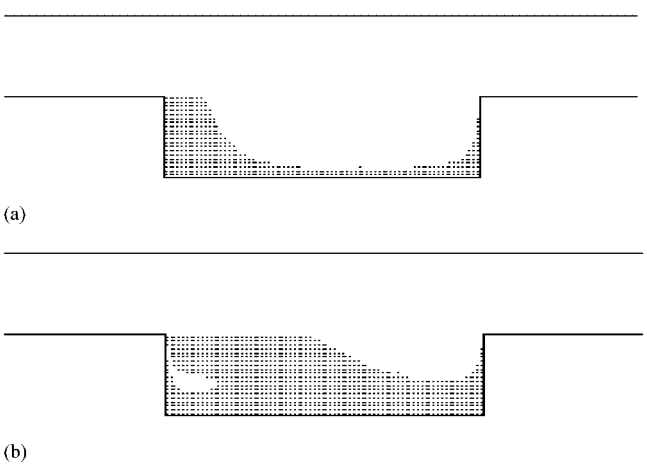

Figure 10. Original layout of markers trapped in the cavity for AR = 4, $Fr = 0.0086$, $Di = 0$ and $Re = 50$. (a) Poiseuille flow and (b) Couette flow.

cavity are displaced with time for Poiseuille duct flow. A vortex is gradually formed after $t = 32$ and, with time, the markers remaining in the cavity are confined in the corners of the cavity. Figure 8, corresponding to Couette duct flow, shows that some of the markers are removed from the cavity at an early stage with most markers remaining in the cavity being caught in the re-circulating regions that develop shortly after the start-up of the duct flow. The distribution of markers remaining in the cavity is depends on the type of duct flow. This is illustrated by Figure 9 which shows the path a particle follows for each type of duct flow. The paths are different and hence the distribution of contaminant is expected to be different. Figure 10 shows the original positions of those markers which remain trapped in the cavity after a long time when the rate of marker removal has reduced to zero. It can be seen that for the AR = 4.0 cavity most markers are removed from the upper downstream end of the cavity, with Couette duct flow leaving the most contaminant in the cavity. Figure 11 shows the percentage of markers removed for cavities of different AR. More markers are removed from a cavity as the cavity aspect ratio increases for both Poiseuille flow and Couette flow, but Poiseuille duct flow is more effective for cleaning cavities, almost by a factor of 2.7 over Couette duct flow.

Copyright © 2003 John Wiley & Sons, Ltd.

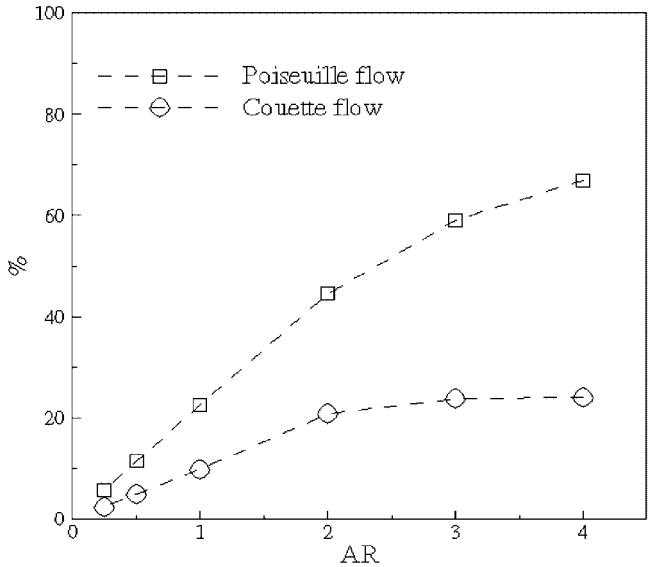

Figure 11. Percentage of markers removed from the cavity for Poiseuille flow and for Couette flow. AR = 4, $Fr = 0.0086$, $Di = 0$ and $Re = 50$.

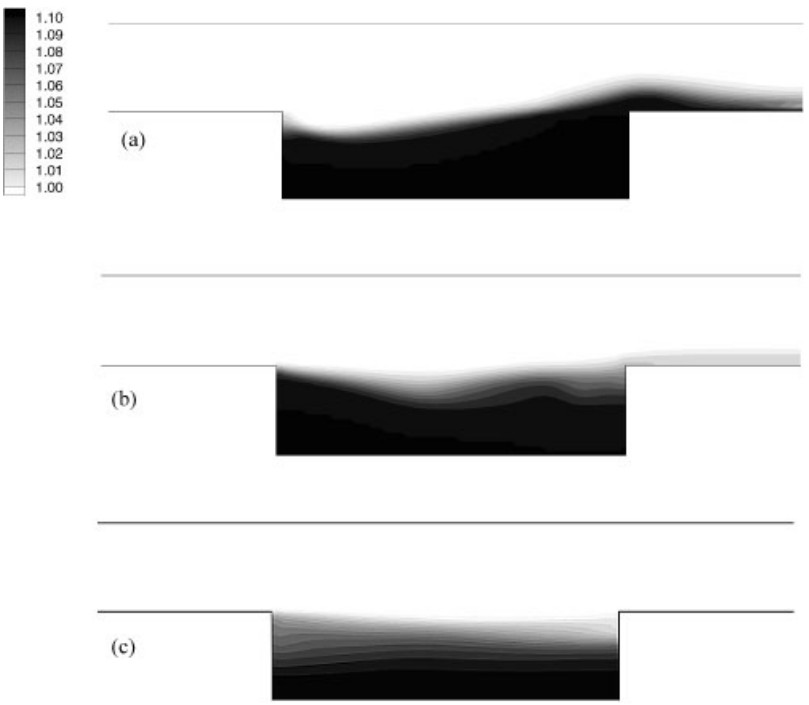

Figure 12. Iso-density contours corresponding to Poiseuille flow over a cavity. AR = 4, $Fr = 0.2781$, $Di = 8.1 \times 10^{-7}$, $Re = 1600$ and $\rho_c = 1.10$. (a) $t = 6$; (b) $t = 48$ and (c) $t = 256$.

Copyright © 2003 John Wiley & Sons, Ltd.

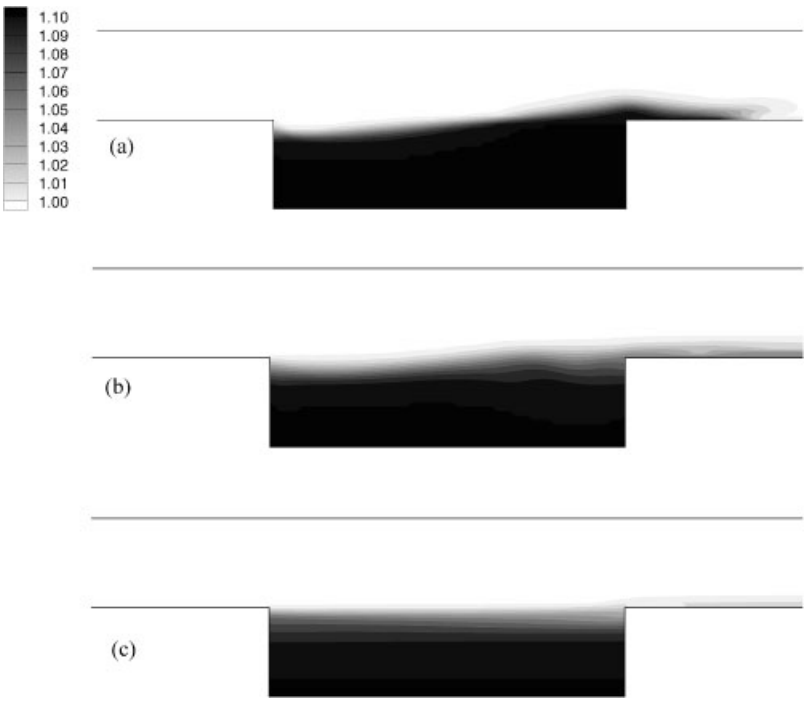

Figure 13. Iso-density contours corresponding to Couette flow over a cavity. AR = 4, $Fr = 0.2781$, $Di = 8.1 \times 10^{-7}$, $Re = 1600$ and $\rho_c = 1.10$. (a) $t = 6$; (b) $t = 48$ and (c) $t = 256$.

3.2. *Case 2: Cavity fluid density greater than duct fluid density*

The problem considered is duct flow over a cavity containing a salt solution of uniform density, while fresh water flows in the duct. Density contours for Poiseuille flow over a cavity with an aspect ratio AR = 4.0, cavity fluid density $\rho_c = 1.10$ and duct flow Reynolds number $Re = 1600$ are shown in Figure 12. For the two-fluid case, like the single fluid case, the duct fluid penetrates into the cavity during the early stages of the flow start-up, thereby removing an amount of cavity fluid. Soon after this initial phase an intermediate layer forms between the duct fluid and the cavity fluid due to diffusion and mixing that takes place. This layer is stratified, having a smoothly varying density distribution, and becomes thicker with time. Stratification inhibits the penetration of the duct flow and therefore reduces the overall removal of markers from the cavity. Since the gravity forces present in a stratified fluid inhibit circulation, it follows that convection-enhanced diffusion is also substantially reduced. Like Poiseuille duct flow, Couette flow (see Figure 13) removes most of the cavity fluid during the early stages of flow development and by $t = 256$ it is clear that the removal rate has decreased substantially, but is still greater than for Poiseuille flow at the same time t. This is due to the greater amount of fluid removed by Poiseuille duct flow during the initial phase making it more difficult to overcome the gravitational forces required to raise the higher density cavity fluid over the step formed by the cavity downstream wall.

Copyright © 2003 John Wiley & Sons, Ltd.

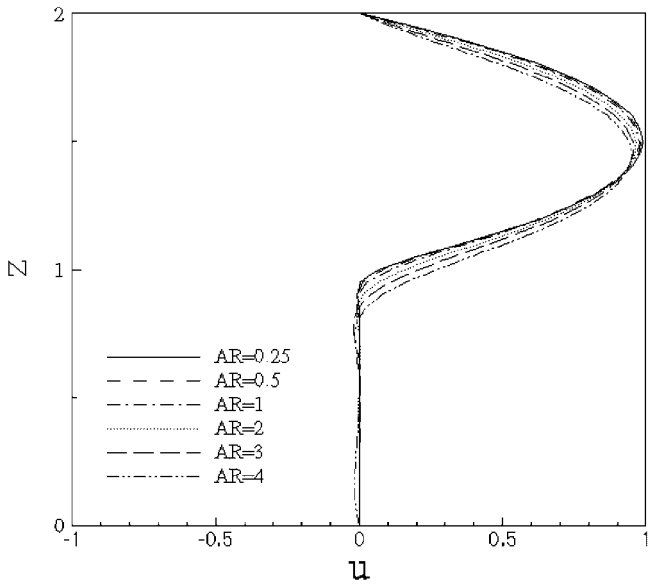

Figure 14. Cavity mid-width normalized velocity profiles at time $t = 256$ for different aspect ratios. Duct flow type: Poiseuille flow. $Fr = 0.2781$, $Di = 8.1 \times 10^{-7}$, $Re = 1600$ and $\rho_c = 1.10$.

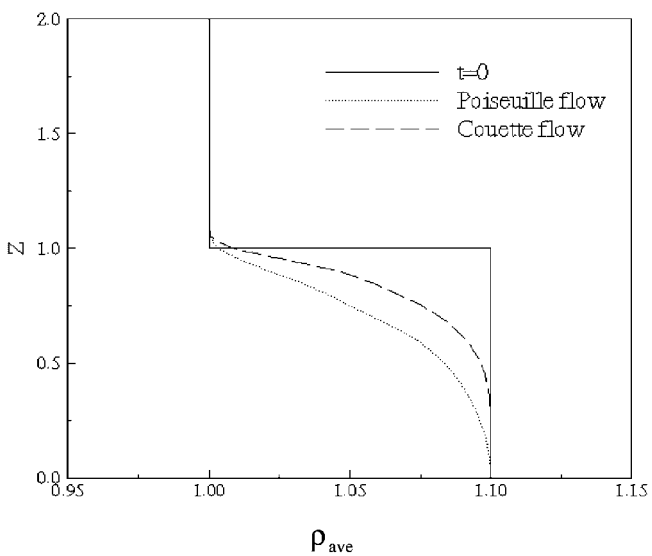

Figure 15. Effect of duct flow type on average normalized density profiles at $t = 256$. AR $= 4$, $Fr = 0.2781$, $Di = 8.1 \times 10^{-7}$, $Re = 1600$ and $\rho_c = 1.10$.

Copyright © 2003 John Wiley & Sons, Ltd.

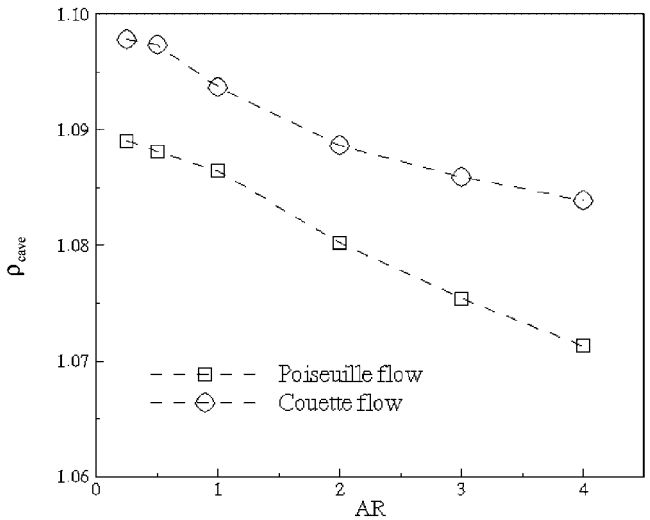

Figure 16. Comparison between Poiseuille flow and Couette flow of the average density in a cavity at $t = 256$. AR $= 4$, $Fr = 0.2781$, $Di = 8.1 \times 10^{-7}$, $Re = 1600$ and $\rho_c = 1.10$.

The velocity profile at the cavity mid-width location shown in Figure 14 indicates the low level of activity in the cavity for this two-density case. For Couette duct flow the stratified layer is not as thick as that created by Poiseuille duct flow. This is shown in Figure 15 where a comparison is made of average normalized density (ρ_{ave}) profiles for a cavity of aspect ratio AR $= 4$ and at time $t = 256$.

An alternative method of quantifying the cleanliness of the cavity fluid is to consider an overall average density for a cavity. The cleanliness of the cavity can be measured by how close the average cavity fluid density is to the duct fluid density. The average cavity fluid density (ρ_{cave}) for Poiseuille and Couette duct flow for a range of AR values is shown in Figure 16, clearly indicating that the higher AR cavities are easier to clean, regardless of the type of flow in the duct, but Poiseuille flow again is more effective at cleaning cavities.

4. CONCLUSIONS

A numerical study of the hydrodynamic cleaning of cavities on the floor of a duct has been carried out for two types of duct flow, Poiseuille flow and Couette flow. For each type of duct flow, the cavity cleaning process has been investigated for cavities containing a fluid with density equal to that of the duct fluid, and for cavities with a miscible fluid of higher density. For the uniform density case and for the two-density case it has been demonstrated that the cleaning process becomes more effective as cavity aspect ratio increases; with Poiseuille duct flow being overall more effective than Couette duct flow. The two-density case is much more difficult to clean because the cavity fluid quickly becomes a diffuse stratified layer which inhibits duct fluid penetration as well as convection-enhanced diffusion. The rate of cleaning is high during the initial stages of the flow start-up and rapidly decreases thereafter.

Copyright © 2003 John Wiley & Sons, Ltd.

REFERENCES

1. Takematsu M. Slow viscous flow past a cavity. *Journal of the Physical Society of Japan* 1966; **21**:1816–1821.
2. Mehta U, Lavan Z. Flow in a two-dimensional channel with a rectangular cavity. *Transactions of the ASME, Journal of Applied Mechanics* 1969; **36**:897–901.
3. O'Brien V. Closed streamlines associated with channel flow over a cavity. *Physics of Fluids* 1972; **15**: 2089–2097.
4. Shen C, Floryan JM. Low Reynolds number flow over cavities. *Physics of Fluids* 1985; **28**:3191–3202.
5. Higdon JL. Stokes flow in a arbitrary two-dimensional domains: shear flow over ridges and cavities. *Journal of Fluid Mechanics* 1985; **159**:195–226.
6. Taneda S. Visualization of separating Stokes flows. *Journal of the Physical Society of Japan* 1979; **46**: 1935–1942.
7. Pozrikidis C. Shear flow over a plane wall with an axisymmetric cavity or a circular orifice of finite thickness. *Physics of Fluids* 1994; **6**:68–79.
8. Kang IS, Chang HN. The effect of turbulence promoters on mass transfer-numerical analysis and flow visualization. *International Journal of Heat and Mass Transfer* 1982; **25**:1167–1181.
9. Kim J, Moin P. Application of a fractional-step method to incompressible Navier–Stokes equation. *Journal of Computational Physics* 1985; **59**:308–323.
10. Chang HN, Ryn HW, Park DH, Park YS. Effect of external laminar channel flow on mass transfer in a cavity. *International Journal of Heat and Mass Transfer* 1987; **30**:2137–2149.
11. Alkire JK, Reiser DB. Effect of fluid flow on removal of dissolution products from small cavities. *Journal of the Electrochemical Society* 1984; **131**:2795–2800.
12. Alkire JK, Deligianni H. The role of mass transport on anisotropic electrochemical pattern etching. *Journal of the Electrochemical Society* 1988; **135**:1093–1100.
13. Yeckel A, Middleman S, Klumb LA. The removal of thin film from periodically grooved surfaces by an impinging jet. *Chemical Engineering Communications* 1990; **96**:69–79.
14. Mickaily ES, Middleman S, Allen M. Viscous flow over periodic surfaces. *Chemical Engineering Communications* 1992; **117**:401–414.
15. Fang LC, Cleaver JW, Nicolaou D. Transient removal of a contaminated fluid from a cavity. *International Journal of Heat and Fluid Flow* 1999; **20**:605–613.
16. Chilukrishna R, Middleman S. Circulation, diffusion, and reaction within a liquid trapped in a cavity. *Chemical Engineering Communications* 1983; **22**:127–138.
17. Harlow FH, Welch JE. Numerical calculation of time-dependent viscous incompressible fluid with free surface. *Physics of Fluids* 1965; **8**:2182–2189.
18. Miyata H, Nishimura S. Finite-difference simulation of nonlinear ship waves. *Journal of Fluid Mechanics* 1985; **157**:327–357.
19. Liu R, Nicolaou D, Stevenson TN. Waves from an oscillatory disturbance in a stratified shear flow. *Journal of Fluid Mechanics* 1990; **219**:609–619.
20. Nicolaou D, Garman JFR, Stevenson TN. Internal waves from a body accelerating in a thermocline. *Applied Scientific Research* 1995; **55**:171–186.
21. Nicolaou D, Liu R, Stevenson TN. The evolution of sheared and nonsheared thermocline waves from an oscillatory disturbance. *Journal of Fluid Mechanics* 1993; **254**:401–416.
22. Chorin AJ. Numerical solution of the Navier–Stokes equations. *Mathematics of Computation* 1968; **22**: 745–762.
23. Viecelli JA. A computing method for incompressible flows bounded by moving walls. *Journal of Computational Physics* 1971; **8**:119–143.
24. Welch JE, Harlow FH, Shannon JP, Daly BJ. The MAC method—a computing technique for solving viscous, incompressible, transient fluid-flow problems involving a free surface. *Los Alamos Scientific Laboratory Report* LA-3425, Los Alamos, 1966.

Copyright © 2003 John Wiley & Sons, Ltd.